



CHORUS

This is the accepted manuscript made available via CHORUS. The article has been published as:

Control of spin-wave emission from spin-torque nano-oscillators by microwave pumping

Vladislav E. Demidov, Sergei Urazhdin, Vasyl Tiberkevich, Andrei Slavin, and Sergej O. Demokritov

Phys. Rev. B **83**, 060406 — Published 22 February 2011

DOI: [10.1103/PhysRevB.83.060406](https://doi.org/10.1103/PhysRevB.83.060406)

Control of spin-wave emission from spin-torque nano-oscillators by microwave pumping

Vladislav E. Demidov¹, Sergei Urazhdin², Vasyl Tiberkevich³, Andrei Slavin³, and Sergej O. Demokritov^{1a)}

¹*Institute for Applied Physics, University of Muenster, Corrensstr. 2-4, 48149 Muenster, Germany*

²*Department of Physics, West Virginia University, Morgantown, WV 26506, USA*

³*Department of Physics, Oakland University, Rochester, MI, USA*

We demonstrate that microwave pumping of a spin-torque nano-oscillator can lead to transfer of the spin-wave energy generated by the oscillator into a mode with frequency given by the difference between the pumping frequency and that of the auto-oscillation. The decay length of spin waves at the combination frequency is significantly increased, while the directionality of emission is preserved. The observed phenomenon provides a route for the implementation of nano-sized spin-wave emitters with controllable emission characteristics for applications in next-generation microwave electronic devices.

PACS numbers: 85.75.-d, 75.40.Gb, 75.30.Ds, 75.75.-c

a) Corresponding author, e-mail: demokrit@uni-muenster.de

It is now well established that spin-polarized electric current injected into a ferromagnetic layer through a nanocontact exerts spin-torque on the magnetization, resulting in microwave-frequency precession [1-9] and emission of spin waves [1,2,10,11]. These current-induced phenomena have been recently intensively studied because of their potential applications in high-frequency microelectronics. In particular, they provide a way for the implementation of tunable nanoscale microwave oscillators, the so-called spin-torque nano-oscillators (STNOs), which can also be utilized as directional steerable sources of spin-waves [11] and ultrasensitive microwave detectors [12] for technical applications within the paradigm of spin-wave logic [13] and nano-optics [14]. Besides these applications, STNOs are fundamentally interesting as strongly nonlinear dynamical systems that exhibit a number of basic nonlinear phenomena. One of such phenomena extensively studied in recent years is the nonlinear interaction of STNOs with external microwave signals [15-20]. This interaction can result in synchronization of STNOs, which can be used to improve their oscillation characteristics. Moreover, precise analysis of the nonlinear synchronization characteristics can also provide additional information about the physical processes in STNOs that are not accessible by other means [19].

Since external microwave signals affect the oscillation of STNOs, one can expect that they also affect the spin-wave emission by STNOs into the surrounding magnetic film. Such effects would be important for the implementation of magnetic devices utilizing spin-wave emission for nanoscale transmission and processing of microwave-frequency signals [13,14,21]. In spite of a significant amount of experimental work, these phenomena have not yet been demonstrated, mainly because of the technical difficulty of the experimental detection of spin waves on the nanoscale. Only very

recently the progress in spatially resolved detection of spin waves has made such measurements possible [11].

In this Letter, we report on the study of spin-wave emission by nano-oscillators subjected to the microwave signals, performed by the spatially resolved micro-focus Brillouin light scattering (BLS) spectroscopy technique [22]. In addition to the previously reported parametric synchronization of STNOs to the microwave pumping signal [19], we demonstrate a phenomenon of pumping-induced spin-wave frequency conversion. This nonlinear dynamical process enables a controllable transfer of energy of the auto-oscillation into the spectral region characterized by lower spatial attenuation of spin waves, resulting in a significant increase of their propagation length. Moreover, we show that this mechanism preserves the unique directionality of the spin-wave emission by the STNO, which makes it promising for application of nano-oscillators as directional steerable spin-wave emitters.

The layout of the experiment is shown in Fig. 1(a). The samples were fabricated by a multistep e-beam lithography process, as follows. A multilayer Cu(40)Py(6)Cu(3)Co₇₀Fe₃₀(9)Au(5), where Py=Ni₈₀Fe₂₀ and thicknesses are given in nanometers, was deposited on a sapphire substrate with electrical leads patterned into coplanar microstrip lines. The top part of the multilayer down to the Py(6) layer was patterned by Ar ion milling through an evaporated Au(70) mask shaped as a 150 nm by 30 nm ellipse, while the bottom electrode and the Py(6) layer were left extended. A SiO₂(40) was subsequently sputtered to electrically isolate the sample leads. The SiO₂ insulator was removed from the Au mask by ion milling with Ar beam nearly parallel to the sample surface, followed by sputtering of an Au(200) top electrode. Thus, the nanopatterned CoFe “polarizing” layer and the Cu spacer formed an elliptical

nanocontact on the extended “free” Py(6) layer with lateral dimensions of 5 by 10 μm . The nanocontact was positioned at a distance of 200 nm from the edge of the top electrode, and its major axis was oriented at 45° with respect to the axis of the electrode. The samples were magnetized by a static in-plane magnetic field $H_0=700$ Oe applied along the top electrode, which produced a non-collinear magnetization configuration of the polarizing and the free layers. The spatially resolved detection of spin waves in the Py film was performed by the micro-focus BLS technique described in detail elsewhere [22]. The probing laser light at the wavelength of 532 nm and power of 1 mW was focused onto the surface of the film and scanned in the two lateral directions, while recording the BLS intensity proportional to the local intensity of spin waves. This technique provided two-dimensional spin-wave intensity maps with a spatial resolution of 250 nm.

For the initial characterization of the dynamical properties of STNO in the absence of external microwave signals, we utilized spectroscopic measurements of the microwave-frequency voltage across the device produced by the fluctuations of the magnetization due to the magnetoresistance [6] [Figs. 1(b),(c)]. Figure 1(b) shows the color-coded map of the dependence of the power spectral density generated by the STNO on the frequency and on the applied dc bias current I . Positive current is defined by the electron flow from the free Py layer to the CoFe polarizer [3-11]. In agreement with the findings of Ref. [11] for the same magnetic configuration of a similar point contact device, the frequency of the auto-oscillation f_0 is nearly independent of I . We determined the amplitude of the oscillations in the nanocontact area from the total microwave power under the oscillation peak normalized by the square of the dc bias

current [Fig. 1 (c)]. Above the oscillation onset at $I \approx 2.7$ mA, the amplitude grows monotonically with I .

Next, we utilized BLS to characterize the emission of spin waves by the STNO into the surrounding Py film, in the absence of external microwave signals. Figure 2(a) shows the BLS spectra of spin waves in the Py film acquired with the probing laser spot positioned close to the edge of the top electrode. The shaded area shows the spectrum acquired at $I=0$, which characterizes the spectral amplitudes of thermally excited spin waves. At $I > 2.7$ mA, the BLS spectra exhibit an additional peak caused by the spin waves emitted by the STNO. The intensity of the peak increases monotonically with the dc bias current, in agreement with the data of Fig. 1(c).

To determine the effects of external microwave signals on the spin wave emission, we applied a “pumping” microwave current at frequency f_p , in addition to the dc bias current I using a bias-T. In all the measurements described below, the applied microwave power was $P=1$ mW. The measurements revealed two qualitatively different regimes depending on the value of f_p , as illustrated in Fig. 2(b). At $f_p = 2f_0 = 14.3$ GHz, the microwave pumping leads to an approximately two-fold increase of the intensity of the auto-oscillation peak, which is indicative of the synchronization of STNO to the external microwave signal with synchronization index $f_p/f_0=2$ [19]. In contrast, at a larger pumping frequency $f_p=15.0$ GHz, the intensity of the auto-oscillation peak decreases and its frequency is slightly reduced. Moreover, a second peak appears in the spectrum at a frequency different from both f_0 and $f_p/2$.

To quantify this phenomenon, we measured the BLS spectra for f_p varying from 13.0 to 17.0 GHz with a step size of 0.1 GHz. These spectra were analyzed to extract the frequency f_1 of the auto-oscillation peak and the frequency f_2 of the secondary peak

induced by the microwave pumping [Fig 3(a)], as well as their intensities J_1 and J_2 [Fig 3(b)]. We identify three regimes in these data, characterized by different behaviors of the frequencies and the intensities of the peaks. In the first regime at $f_p < 13.8$ GHz there is only one peak in the spectrum whose frequency $f_1 \approx 6.9$ GHz is nearly independent of f_p . In the second regime, in the range $13.8 \text{ GHz} < f_p < 14.4 \text{ GHz}$, there is still only one peak, but its frequency follows an exact linear relationship with the pumping frequency, $f_1 = f_p/2$. This behavior is consistent with the synchronization of the STNO to the pumping signal characterized by the synchronization index $f_p/f_1 = 2$. The frequency range of the synchronized regime is determined predominantly by the nonlinear characteristics of the STNO [19]. In the third regime, at f_p above the upper boundary of the synchronized regime at 14.4 GHz, a second peak with frequency f_2 appears in the spectrum, while the frequency f_1 of the first peak abruptly decreases. The frequency f_2 of the secondary peak increases with increasing f_p , whereas f_1 remains unchanged.

We can identify an important correlation between the frequencies f_1 and f_2 of the two peaks and the pumping frequency f_p . Namely, the mean frequency of the peaks $(f_1 + f_2)/2$ shown in Fig. 3(a) by diamonds is equal to $f_p/2$ shown in Fig. 3(a) by a straight line. This observation enables one to associate the generation of the secondary peak with the nonlinear frequency mixing between the microwave pumping and the dynamic magnetization signal generated by the STNO, resulting in the generation of a combinatory spectral harmonic. This process can be also interpreted as the pumping-mediated transfer of the microwave energy generated by the STNO into another frequency range. This explanation is consistent with the decrease of the intensity of the auto-oscillation peak observed simultaneously with the appearance of the secondary peak [Fig. 2(b)]. The suppression of the primary peak is also clearly seen in the

dependencies of the BLS intensities of the peaks on f_p [Fig. 3(b)]. In comparison to the free-running auto-oscillation intensity shown in Fig. 3(b) by a dashed horizontal line, the intensity J_1 of the primary oscillation peak is noticeably suppressed at all pumping frequencies, except for the enhancement in the synchronization region and a less pronounced suppression around $f_p=16$ GHz. We also note that the suppression of the auto-oscillation peak occurs at f_p both *below* and *above* the synchronization region 13.8-14.4 GHz, whereas the secondary peak induced by the pumping appears *only above* 14.4 GHz. To understand why a secondary peak is not observed at $f_p < 13.8$ GHz, we assume that the nonlinear frequency mixing occurs for any pumping frequency outside the synchronization region. However, it can lead to the excitation of propagating spin waves only if the frequency generated by the mixing falls within the spin-wave spectrum of the extended Py film outside the point contact area. Otherwise, the frequency mixing should result in the generation of a non-resonant magnetization oscillation which is localized within the point contact area.

We now address the spatial characteristics of the emitted spin waves in different regimes. Figure 4(a) shows a two-dimensional map of the spin-wave intensity recorded at the auto-oscillation frequency in the absence of pumping. This map is similar to those observed in [11]: the spin-wave emission is strongly directional and occurs in the two opposite directions perpendicular to the static field H_0 . The asymmetry between the emission lobes is associated with the interplay between H_0 and the Oersted field of the dc current. The emitted spin waves exhibit a strong spatial decay. While the map shown in Fig. 4(a) was recorded in the absence of pumping, very similar maps were also observed in the presence of pumping for spin waves corresponding to the auto-oscillation peak at f_1 . Within the entire frequency range $f_p=13-17$ GHz, the spatial decay

of the emitted waves remained unchanged, albeit their intensity varied in accordance with the data of Fig. 3(b).

A different behavior was found for spin waves corresponding to the pumping-induced combinatory frequency f_2 . Their spatial decay length was found to be significantly larger than that for the waves corresponding to the auto-oscillation peak at f_1 . A typical example of the emission patterns corresponding to $f_2=7.99$ GHz ($f_p=15$ GHz) is shown in Fig. 4(b). Comparing the two maps in Figs. 4(a) and 4(b), one can clearly see that the emission induced by the pumping preserves the main features of the emission at the self-oscillation frequency, but is characterized by a noticeably larger spin-wave propagation length. We emphasize that the emission patterns for pumping-induced spin waves exhibit a strong directionality, which cannot be obtained by direct excitation of spin waves by microwave-frequency current [18, 23], and qualitatively distinguishes the two phenomena. This feature makes the observed effect promising for applications of STNOs as directional steerable spin-wave emitters.

Figure 5 shows the intensity of emitted spin waves as a function of the distance from the nano-contact obtained from the emission patterns shown in Fig. 4 by integrating along the direction parallel to H_0 . These dependencies are well described by an exponential decay, as shown by linear fits on the logarithmic scale. The decay is significantly stronger for spin waves at the frequency of the auto-oscillation compared to the waves at the combinatory frequency. From the data of Fig. 5, we obtain the values of the decay lengths: $\xi=540$ nm for the emission at the auto-oscillation frequency $f_1=7.15$ GHz, and $\xi=940$ nm for the pumping-induced emission at $f_2=7.99$ GHz.

To explain the different decay lengths of these two waves, we consider a parabolic approximation for the dispersion of spin waves with wavevectors $\vec{k}=(k_{\parallel}, k_{\perp})$ close to

the position $\vec{k}_{\min} = (k_{\parallel, \min}, k_{\perp, \min}) = (k_{\min}, 0)$ of the minimum spectral point f_{\min} [11]. This approximation is justified by the proximity of the observed oscillation frequencies to the value $f_{\min}=6.9$ GHz estimated from the experiment. The in-plane orientation of the wavevector is defined with respect to the applied magnetic field H_0 . For spin waves propagating perpendicular to H_0 (see Fig. 4) and $k_{\parallel} = k_{\min}$, the spin-wave dispersion can be written as follows:

$$f(k_{\perp}) = f_{\min} + Dk_{\perp}^2, \quad (1)$$

where D is the effective spectral stiffness determined mainly by the strength of the exchange interaction. The wavevector k_{\perp} has a complex value $k_{\perp} = \kappa' + i\kappa''$, where the imaginary part κ'' determines the decay length $\xi = 1/\kappa''$.

To determine the dependence of the decay length on the spin-wave frequency, we consider the waves described by the dispersion relation (1) and the damping rate Γ , which for simplicity is assumed to be independent of frequency. Equation (1) can then be written as

$$f - i\Gamma = f_{\min} + D(\kappa' + i\kappa'')^2. \quad (2)$$

Equation (2) allows one to determine both the real component κ' and the imaginary component κ'' of k_{\perp} . The latter yields the expression for the decay length

$$\xi = \frac{2D}{\Gamma} \left(\frac{\Delta f}{\Gamma} + \sqrt{1 + \left(\frac{\Delta f}{\Gamma} \right)^2} \right), \quad (3)$$

where $\Delta f = f - f_{\min}$. Equation (3) shows that, for a given decay rate Γ , the decay length increases with increasing spin wave frequency f , explaining the observed larger decay length of the high-frequency pumping-induced secondary spin wave. The proposed model is clearly too simple to make a quantitative comparison of Eq. (3) with the

experimental data. Nevertheless, it is instructive to estimate the relevant parameters. By using a typical value $\alpha_G = 0.01$ for the Gilbert constant, we obtain $\Gamma = \alpha_G \gamma (H + 2\pi M) \approx 0.12$ GHz, where $4\pi M = 9.8$ kG is the magnetization of Py and $\gamma = 2.9$ GHz/kG is the gyromagnetic ratio. Using the value $D = 2.5 \times 10^3$ GHz(nm)² for the exchange constant in Py, we obtain $\xi = 430$ nm at $f = 7.15$ GHz and $\xi = 950$ nm at $f = 7.99$ GHz. These values are in a reasonable agreement with the values $\xi = 540$ nm and $\xi = 940$ nm determined from the spatially resolved BLS measurements.

In conclusion, we have demonstrated that microwave pumping can be used not only for the synchronization of STNOs, but also as a mechanism for the transfer of the generated microwave energy into the desirable spectral range. The latter effect enables an increase of the propagation length of spin waves emitted by STNOs. Moreover, we demonstrated that the phenomenon of the pumping-induced emission does not disturb the unique directionality found for the emission in the auto-oscillation regime. These features make the studied phenomenon very promising for applications of STNOs in analog and digital spin-wave-based integrated circuits.

The contribution to this work in Germany was supported in part by the Deutsche Forschungsgemeinschaft and by the European Grant Master (No. NMP-FP7 212257). The work in the USA was supported by NSF DMR-0747609, ECCS-1001815 and ECCS-0967195, the Research Corporation, and the U.S. Army TARDEC, RDECOM (Contracts W56HZV-09-P-L564 and W56HZV-10-P-L687).

REFERENCES

- [1] J. C. Slonczewski, *J. Magn. Magn. Mater.* **159**, L1-L7 (1996).
- [2] L. Berger, *Phys. Rev. B* **54**, 9353-9358 (1996).
- [3] E. B. Myers, D. C. Ralph, J. A. Katine, R. N. Louie, and R. A. Buhrman, *Science* **285**, 867-870 (1999).
- [4] J. A. Katine, F. J. Albert, R. A. Buhrman, E. B. Myers, and D. C. Ralph, *Phys. Rev. Lett.* **84**, 3149-3152 (2000).
- [5] M. Tsoi, A. G. M. Jansen, J. Bass, W.-C. Chiang, V. Tsoi, and P. Wyder, *Nature* **406**, 46-48 (2000).
- [6] S. I. Kiselev, J. C. Sankey, I. N. Krivorotov, N. C. Emley, R. J. Schoelkopf, R. A. Buhrman, and D. C. Ralph, *Nature* **425**, 380-383 (2003).
- [7] S. Urazhdin, N. O. Birge, W. P. Pratt, Jr., and J. Bass, *Phys. Rev. Lett.* **91**, 146803 (2003).
- [8] W. H. Rippard, M. R. Pufall, S. Kaka, S. E. Russek, and T. J. Silva, *Phys. Rev. Lett.* **92**, 27201 (2004).
- [9] I. N. Krivorotov, N. C. Emley, J. C. Sankey, S. I. Kiselev, D. C. Ralph, and R. A. Buhrman, *Science* **307**, 228-231 (2005).
- [10] M. R. Pufall, W. H. Rippard, S. E. Russek, S. Kaka, and J. A. Katine, *Phys. Rev. Lett.* **97**, 087206 (2006).
- [11] V. E. Demidov, S. Urazhdin, and S. O. Demokritov, *Nature Materials* **9**, 984 (2010).
- [12] X. Cheng, C. T. Boone, J. Zhu, and I. N. Krivorotov, *Phys. Rev. Lett.* **105**, 047202 (2010).

- [13] A. Khitun, M. Bao, and K. L. Wang, IEEE Trans. Mag. **44**, 2141 (2008).
- [14] V. E. Demidov, S. O. Demokritov, K. Rott, P. Krzysteczko, and G. Reiss, Appl. Phys. Lett. **92**, 232503 (2008).
- [15] W. H. Rippard, M. R. Pufall, S. Kaka, T. J. Silva, S. E. Russek, and J. A. Katine, Phys. Rev. Lett. **95**, 067203 (2005).
- [16] J. C. Sankey, P. M. Braganca, A. G. F. Garcia, I. N. Krivorotov, R. A. Buhrman, and D. C. Ralph, Phys. Rev. Lett. **96**, 227601 (2006).
- [17] B. Georges, J. Grollier, M. Darques, V. Cros, C. Deranlot, B. Marcilhac, G. Faini, and A. Fert, Phys. Rev. Lett. **101**, 017201 (2008).
- [18] H. Schultheiss, X. Janssens, M. van Kampen, F. Ciubotaru, S. J. Hermsdoerfer, B. Obry, A. Laraoui, A. A. Serga, L. Lagae, A. N. Slavin, B. Leven, and B. Hillebrands, Phys. Rev. Lett. **103**, 157202 (2009).
- [19] S. Urazhdin, P. Tabor, V. Tiberkevich, and A. Slavin, Phys. Rev. Lett. **105**, 104101 (2010).
- [20] S. Urazhdin, V. Tiberkevich, and A. Slavin, Phys. Rev. Lett. **105**, 237204 (2010).
- [21] V.V. Kruglyak, S.O. Demokritov, and D. Grundler, J. Phys. D: Appl. Phys. **43**, 264001 (2010).
- [22] S. O. Demokritov and V. E. Demidov, IEEE Trans. Mag. **44**, 6 (2008).
- [23] V. E. Demidov, S.O. Demokritov, G. Reiss, and K. Rott, Appl. Phys. Lett. **90**, 172508 (2007).

FIGURE CAPTIONS

FIG. 1. (Color online) (a) Schematic of the experiment. Inset shows an SEM micrograph of the device. (b) Pseudo-color logarithmic map of the power spectral density (PSD) of the signal generated by the device due to the magnetoresistance effect in the absence of the external microwave signal. (c) Integral power generated by the device normalized by I^2 vs the dc bias current I .

FIG. 2. (Color online) (a) BLS spectra of spin waves in the Py film in the absence of the external microwave signal, acquired at different values of I , as labeled. The shaded region is the spectrum of thermally excited spin waves acquired at $I=0$. (b) BLS spectra acquired at $I=5$ mA in the presence of an additional microwave current with power $P=1$ mW, applied at the labeled values of frequency f_p . The shaded region shows the reference spectrum acquired in the free-running auto-oscillation regime, at $I=5$ mA.

FIG. 3. (Color online) Dependencies of the frequencies (a) and intensities (b) of the oscillation peaks on the pumping frequency. Circles show the data for the auto-oscillation peak and squares – for the pumping-induced secondary peak. In (a), diamonds show the mean frequency $(f_1+f_2)/2$, and the solid straight line shows $f_p/2$. Dashed horizontal line in (b) is the intensity of the auto-oscillation peak in the absence of the external microwave signal.

FIG. 4. (Color online) Pseudo-color spatial intensity maps of the emitted spin waves, acquired at $I=5$ mA. A schematic of the top electrode and a cross indicating the location of the nanocontact is superimposed on each map. (a) Spin-wave map at the frequency of auto-oscillation, in the absence of the external

microwaves. (b) Spin-wave emission at the frequency of the pumping-induced secondary peak, at $f_p=15$ GHz.

FIG. 5. (Color online) Logarithmic plot of the integral intensity of the emitted spin waves *vs* the distance from the nano-contact. Circles – data for the auto-oscillation regime acquired at the oscillation frequency, squares – data for the pumping-induced nonlinear mixing regime acquired at the frequency f_2 of the secondary peak.

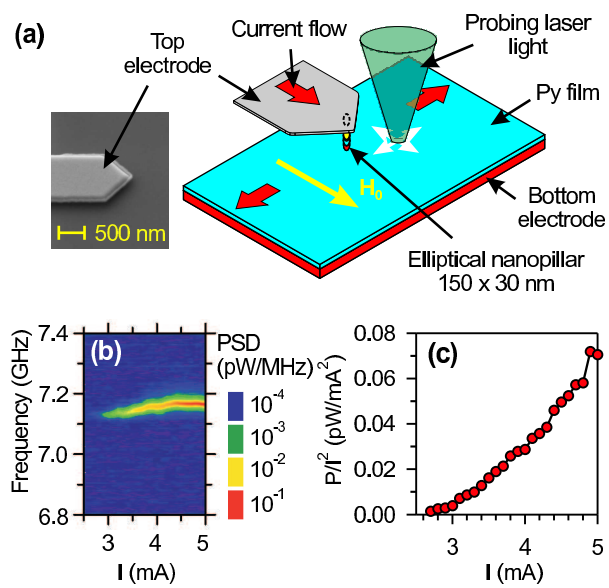
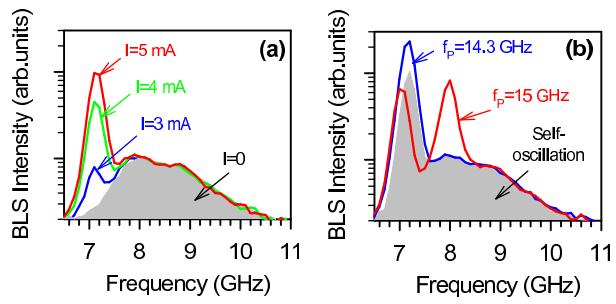


Figure 1 LX12132BR 19JAN2011



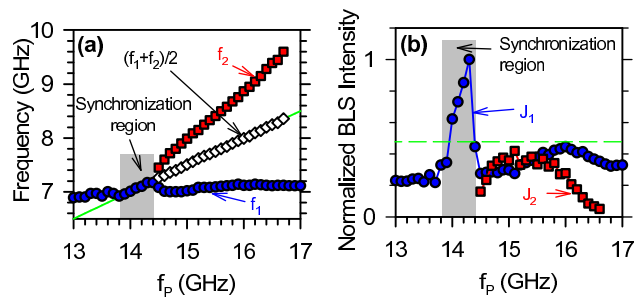
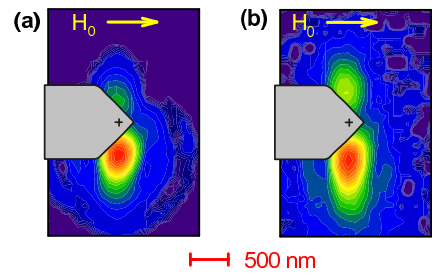


Figure 3 LX12132BR 19JAN2011



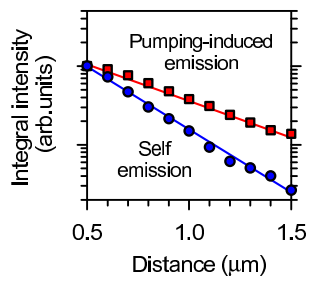


Figure 5

LX12132BR

19JAN2011